Design of Inspection Robot for Spherical Tank Based on Mecanum Wheel

Jie LI[1], Huang Feng[1],Chun-lei Tu[1,2], Shan-shan JIN[1],Xing-song WANG[1]

[1]*College of Mechanical Engineering, Southeast University, Nanjing, China*

[2]*Special Equipment Safety Supervision Inspection Institute of Jiangsu Province, Nanjing, China*

xswang@seu.edu.cn

Abstract: Traditional manual weld inspection of large spherical tank has high cost, low efficiency and high degree of danger. It is of great significance to design an automated weld flaw detection system. This paper designs a wheeled wall-climbing robot that can crawl on the outer wall of the spherical tank. The Mecanum wheeled trolley is used as a mobile platform for ultrasonic testing with ultrasonic testing equipment. Firstly, the key structure of the robot is introduced, and the independent suspension structure and spherical adjustment mechanism are designed. The reliability of magnetic adsorption was analyzed by static calculation, and the rationality of the structure was verified. The ultrasonic probe fixture is designed according to the ultrasonic flaw detection process. The defect size calculated according to the flaw detection principle. Through the experiment, the motion effect of the wall-climbing robot on the curved surface is analyzed, and the rationality and application value of the wall-detecting robot flaw detection scheme are verified.

Keywords: climbing robot; weld inspection of spherical tank; mecanum wheel; ultrasonic inspection

1 Introduction

Spherical tanks, as a common pressure vessel, are widely used for the storage of various dangerous goods media. Due to the special nature of its storage media, its security performance needs to be checked regularly. The weld is a weak part of the spherical tank, which is prone to defects and poses great safety hazards. Therefore, it is necessary to periodically test the spherical weld of the spherical tank. The volume of the large spherical tank shown in Figure 1 is 2000 cubic meters. It needs to be opened every three years. The tank can be shut down for 3-5 months. After the defect is repaired, it needs to be tested twice. It is of great significance to design an automated weld flaw detection system [1, 2].

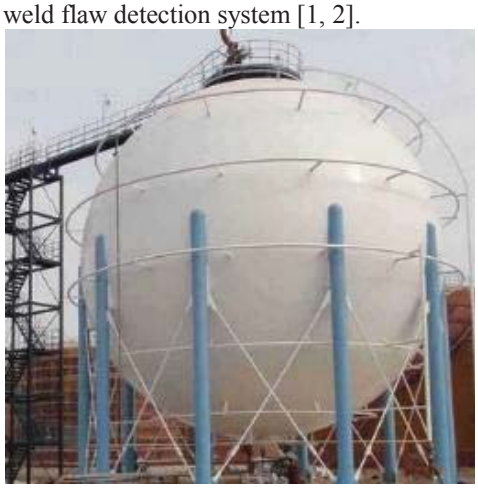

Figure 1. Industrial large spherical tank

978-1-7281-3410-9/19/$31.00 ©2019 IEEE

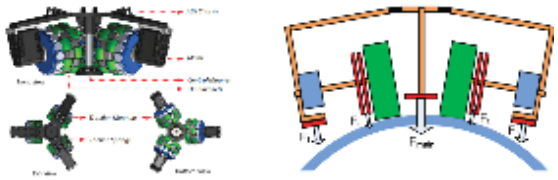

Figure 2. Magnetic sorption wall climbing robot

From the current international and domestic technology status, wall testing automation equipment mostly uses wall climbing robots [3-6]. The University of Coimbra has developed an omnidirectional moving wheel magnetic sorption wall climbing robot [7], as shown in Figure 2. The robot has adopted an omnidirectional moving wheel, and the main advantage is that it can be used to improve the mobility of the mobile robot.

This paper designs a detection robot, which replaces the original manual detection method and detects the weld seam of the spherical tank without opening the can. Due to the risk of high-altitude operations, dangerous goods leakage, and detection equipment radiation, the detection robot can protect the personal safety of the inspection personnel and greatly reduce the risk. Compared with manual repetitive work, the robot performs mechanical repetitive work under the established programming, which can be well protected in terms of efficiency and quality.

2 Design of the Robot Structure

2.1 Overall Structure of the Robot

Authorized licensed use limited to: Massey University. Downloaded on August 08,2020 at 23:15:40 UTC from IEEE Xplore. Restrictions apply.

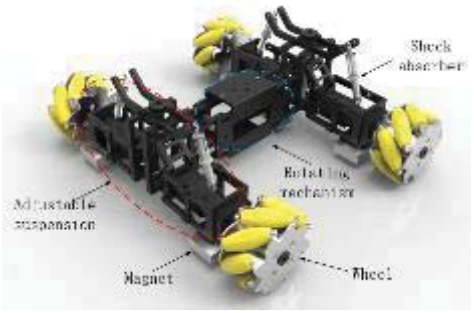

Figure 3. 3D modeling of the robot

The main body of the detection robot designed in this paper is a wheeled wall-climbing robot. The part equipped with the detection equipment is a car structure based on Mecanum wheels [8, 9], and uses magnetic adsorption, as shown in Figure 3.

The Mecanum wheel is a four-wheel drive. It requires four wheels to make good contact with the wall when climbing the wall. Therefore, the robot design requires an adjustment mechanism to adapt to the spherical creep of different curvatures. The suspension is designed to adjust the independent suspension structure, and the angle between the same row of wheels can be adjusted by adjusting the top knob. The relative posture of the front and rear suspensions can be adjusted by an intermediate rotation mechanism. Suspension adjustment and adjustment of the intermediate rotating mechanism ultimately allows the car to adapt to the surface of the can. The shock absorber is used for surface adaptation.

2.2 Adjustable Independent Suspension

The Mecanum car needs four wheels to cling to the ground when moving. The suspension enables the car to overcome obstacles such as welds on the surface of the tank, reducing the vibration of the robot during exercise. When an obstacle is encountered, the independent suspension is deformed so that the wheel can overcome the obstacle alone, thereby reducing the impact on other drive wheels.

The structure of the robot suspension designed to adapt the wheels to the surface crawling is shown in Figure 4. The adjusting knob is fixedly connected to the long stud, and the adjusting slider has an internal thread and is mounted on the stud. The adjustment slider is hinged to the suspension on both sides by a parallelogram mechanism link. By rotating the adjustment knob, the attitude change of the four wheels in space can be realized, and the axial direction of each wheel is perpendicular to the normal of the spherical surface. At this time, the distance between the magnet and the curved surface is also consistent, so that each wheel is close to the spherical surface, and each wheel can output power. In addition to the four-wheels, the suspension structure can be completely adjusted to the wall surface by a certain adaptive adjustment. When the obstacles such as the weld seam are crossed, the wheels contacting the obstacles are lifted independently, and the other wheels and the curved surface are not affected. Since the

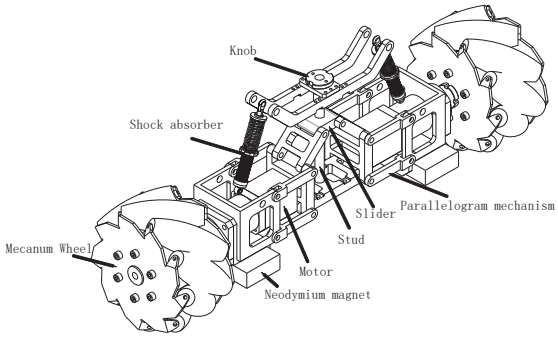

Figure 4. Adjustable independent suspension structure

relative position of the magnet and the wheel of the obstacle is kept constant, the interference of the magnet with the obstacle is avoided. At the same time, the suction force of the magnet on the wall of the spherical tank is not changed, thereby increasing the safety of climbing.

2.3 Ultrasonic Probe Clamping Mechanism

Ultrasonic flaw detection equipment needs to be mounted on the car according to the design requirements, and move along the weld along the trolley. Because the spherical tank has a certain curvature, when the surface is attached to the curved surface, the symmetrically arranged chucks on both sides of the welded seam have a certain angle with each other, and a certain mechanism is required to clamp the probe, which can adapt to the spherical can of different curvatures.

In order to meet the flaw detection process, the probe needs to be closely attached to the spherical tank. The clamping mechanism needs a certain amount of deformation when the ultrasonic probe is clamped on the wall surface, so as to ensure a good fit between the probe and the surface of the measured spherical tank. According to the shape parameters of the ultrasonic probe, the probe fixture is designed as shown in Figure 5. The clamp chuck portion has a rotating joint, which allows the posture of the chuck to be ±3°. The support frame is connected to the frame through two long holes, and the long hole provides a displacement deformation allowance of 4 mm in the vertical direction of the clamp. The hole adjacent to the long hole has a tension spring mounting position, and is connected to the main body of the robot to provide a pressing force to the probe.

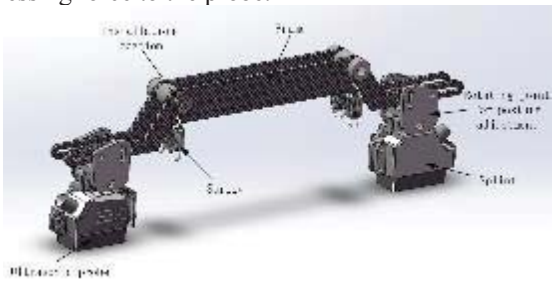

Authorized licensed use limited to: Massey University. Downloaded on August 08,2020 at 23:15:40 UTC from IEEE Xplore. Restrictions apply.

Figure 5. Model of ultrasonic probe

3 Robot Structure Analysis and Defect size Calculation

3.1 Analysis of the Suspension on Curvature Adaptation

Due to the presence of the adjustment knob, adjusting the suspension allows for convenient adjustment of the wheel attitude to achieve wall adaptation to different curvatures. Figure 6 shows the limit position of the state and posture when the suspension is attracted to the spherical surface.

The ideal working state is: adjusting the slider EF up and down by the knob to change the wheel posture, so that each wheel is axially perpendicular to the spherical normal. The wheel portion is connected to the frame by a parallelogram mechanism, and the direction GH indicating the posture of the wheel is kept parallel to the AB link in the frame. Since the vehicle width b is small with respect to the radius R of the spherical tank, the attitude angle α can be equaled as:

$$\alpha = \frac{180}{\pi} \arctan \frac{W}{R} \tag{1}$$

Figure 7 shows the suspension attitude adjustment structure. The adjusting knob is fixed to the stud by the pin, the pitch of the stud is 1.5mm, and the positioning hole of the knob is reserved for fixing the adjusted position, so the adjustment index of the adjusting slider in the vertical direction is 0.375mm.

The specific length of the connecting rod brought into the frame, the analysis rod AB and CD calculate the relative position of each rod in the matlab with the movement of the adjusting slider, and draw the posture space adjusted by AB and CD rod as shown in Figure 8. The angle of variation with the vertical direction ranges from -25.9° to 22.8°. Bringing the angle adjustment range into equation (1) allows the suspension to accommodate a spherical radius of curvature R of at least 1.12 m.

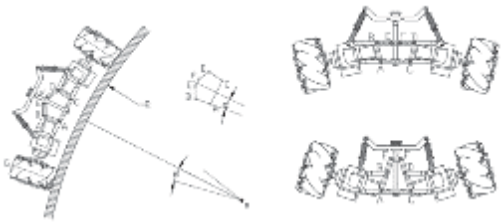

Figure 6. Working status of suspension

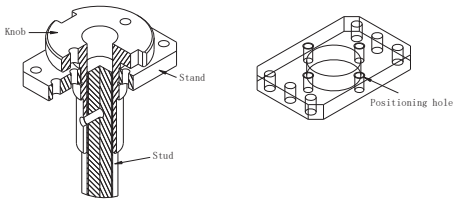

Figure 7. Suspension posture adjustment stud

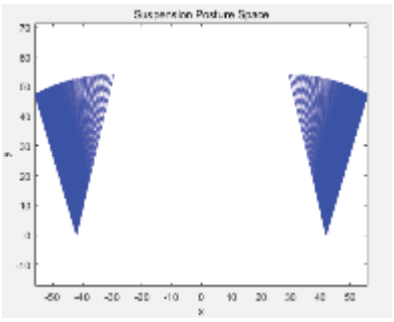

Figure 8. Suspension posture space

3.2 Magnetic Adsorption Capacity Analysis

As the adsorption force, the magnetic force needs to be large enough to meet the safety adsorption. However, the excessive magnetic force will increase the resistance of the robot to crawl. Therefore, the magnetic adsorption force needs to be analyzed, so that the magnet can reduce the redundancy that hinders the movement of the car on the basis of stable adsorption. The remaining suction minimizes the power consumption of the robot.

As shown in Figure 9, when the crawler is stationary on the wall, it is assumed that the magnets attached to the four wheels are all F_m, analysis of the overall force is available:

$$\begin{cases} 4F_m \cos\beta = 2(F_{f12} + F_{f34})\sin\beta + \\ \qquad 2(F_{N12} + F_{N34})\cos\beta \\ G_t + 2(F_{N12} + F_{N34})\sin\beta = 4F_m \sin\beta + \\ \qquad 2(F_{f12} + F_{f34})\cos\beta \end{cases} \tag{2}$$

$$G_t L\cos\beta + 4F_{N12}L = 4F_m L \tag{3}$$

The change in attitude of the crawler on the wall affects the direction of magnetic force and friction. There are two limit states:

1) $\beta = 0°$, below the water level, the adsorption force needs to overcome the robot's own weight to prevent falling, need to meet:

$$4F_m > G_t \tag{4}$$

Authorized licensed use limited to: Massey University. Downloaded on August 08,2020 at 23:15:40 UTC from IEEE Xplore. Restrictions apply.

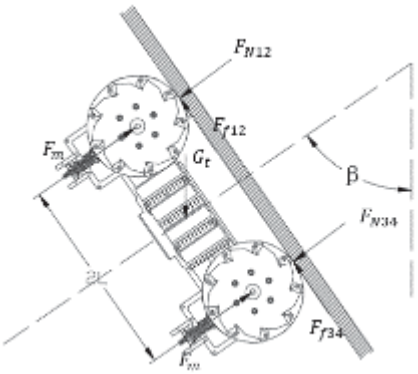

Figure 9. Overall force diagram of the robot

2) $\beta = 90°$, in the vertical wall, the positive pressure on the wall is equal to the adsorption force, and the maximum static friction needs to overcome the gravity of the robot to prevent the slip.

$$4\mu F_m > G_t \tag{5}$$

Take the maximum static friction coefficient μ as 0.4, The total weight of the robot (G_t) is 250N, then the magnetic force F_m>156.25N

The magnet used was an industrial grade neodymium magnet and the material is NdFeB. The performance parameters are shown in Table 1.

According to the gap between the independent magnet and the tank wall, the magnetic field force distribution of the magnet is simplified, and the magnet is magnetized in one direction along the long side. The magnetic equation can be approximated by the following formula [5]:

$$F = \frac{\mu_r - 1}{2\mu_0 \mu_r} B^2 S = \frac{1}{2\mu_0} B^2 S \tag{6}$$

The simulation results of the magnetic force using Ansys Maxwell are shown in Figure 10. It can be seen from the simulation that the magnetic force is more evenly distributed in the center of the magnet, and there is a concentrated magnetic line at the edge of the magnet. The magnetic attraction force of a single magnet perpendicular to the tank wall provided at 4 mm from the tank wall is 225.96 N. Similarly, the magnet is placed parallel to the wall surface, and the distance from the center of the magnet to the wall surface is adjusted. The magnitude of the magnetic force simulated by the simulation is shown in Figure 11.

Table 1. Permanent Magnet Parameter

category	parameter
Type	N52
Residual magnetic induction （mT）	1430-1480
Shape parameter （mm）	100x50x20
Coercivity （kA/m）	＞796
Intrinsic coercivity （kA/m）	＞876
Maximum magnetic energy （kJ/m^3）	398-422

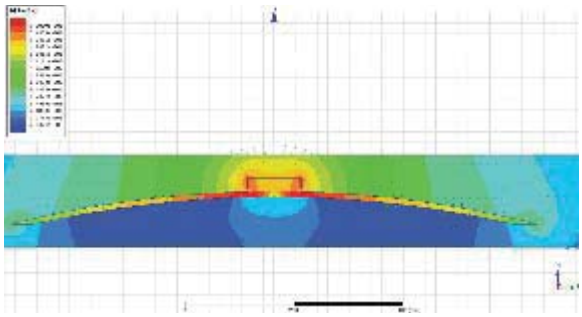

Figure 10. Magnetic simulation of a single magnet

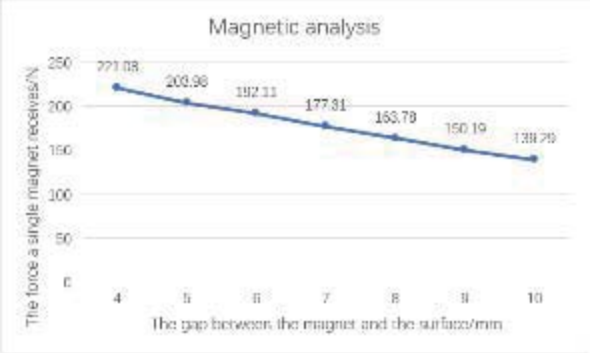

Figure 11. Magnetic analysis of single magnet

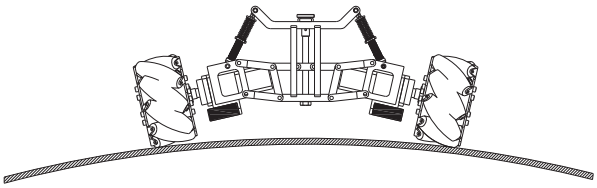

Figure 12. Highest position of the suspension

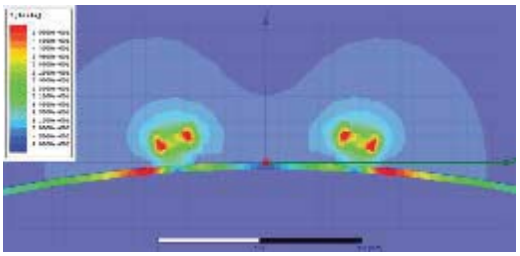

Figure 13. Magnetic simulation of the highest position

Four neodymium magnets are used in the robot structure to ensure the stability of magnetic adsorption but make it difficult to remove the robot from the wall. The suspension structure designed in this paper can adapt to different curvatures on the one hand. On the other hand, the knob can be adjusted to increase the distance of the magnet from the wall surface, and the adsorption force to be overcome by removing the robot from the wall surface is reduced.

Authorized licensed use limited to: Massey University. Downloaded on August 08,2020 at 23:15:40 UTC from IEEE Xplore. Restrictions apply.

Taking the wall surface creeping condition of the experimental platform 4m diameter 10mm wall thickness as an example, Figure 12 shows the highest position of the suspension obtained according to Section 3.1. The magnetic force simulation is carried out with reference to the positional relationship as shown in Figure 13. From the simulation, the total adsorption force of the four magnets on the wall surface is 219.1N, which is roughly one quarter of the working state of the robot, and it is convenient to remove the crawler from the wall surface after the shutdown.

3.3 Analysis of Moving Capability on Crossing Obstacles

There are obstacles including welds on the surface of the spherical tank. To ensure that the robot can work smoothly, the robot needs to have certain obstacles. As shown in Figure14, when the trolley encounters an obstacle, the shock spring is deformed, and the obstacle wheel is lifted independently to overcome the obstacle, and does not affect the driving of the other wheels. Therefore, the suspension spring needs a certain pre-tightening force during installation. If the pre-tightening force is too small, the overall rigidity of the frame will not be guaranteed. If the pre-tightening force is too large, the obstacle performance of the trolley will be affected. Figure 15 is a force diagram of the suspension over the obstacle and the deformation, and the spring preload force required for the trolley installation is analyzed and calculated.

Under ideal conditions, when the trolley stands on the wall in a positive posture, the gravity G_f of the suspension bearing frame does not deform, and the preload force P_0 of the spring satisfies the formula:

$$4P_0 \sin\theta \geq G_f \tag{7}$$

When the single wheel of the trolley crosses the obstacle with a height of Δh, the amount of spring deformation is Δh/sinθ. In the ideal obstacle state, the wheel that encounters the obstacle is lifted independently, and the remaining wheels remain in the same posture, so the remaining wheels and the frame are regarded as In the rigid body calculation, assuming that the magnetic force (F_m) is concentrated on the center of the magnet, the spring force (P_1) of the suspension where the wheel is lifted satisfies the relationship:

$$\begin{cases} P_1 = P_0 + \dfrac{k\triangle h}{\sin\theta} \\ P_1 \sin\theta(l_p + l_w) + P_1 \cos\theta h_p \\ \leq 2F_m(l_w - l_m) + F_m(l_w + l_m) + G_f l_w \end{cases} \tag{8}$$

The preload force (P_0) of the spring satisfies the formula:

$$\frac{G_f}{4\sin\theta} \leq P_0 \leq \frac{(3F_m + G_f)l_w - F_m l_m}{(l_p + l_w)\sin\theta + h_p \cos\theta} - \frac{k\triangle h}{\sin\theta} \tag{9}$$

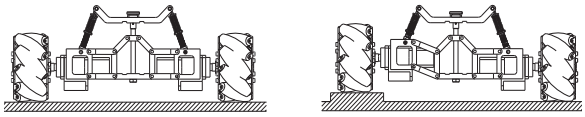

Figure 14. Deformation diagram of crossing obstacles

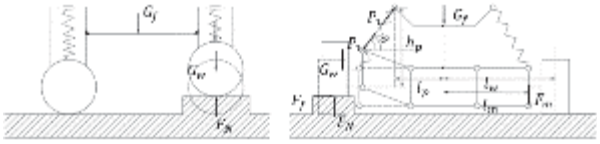

Figure 15. Static analysis of crossing obstacle

Table 2. Robot Prototype and Weld Parameter

Symbol	Units	Value
G_f	N	83
l_w	mm	237
l_m	mm	135
F_m	N	204
l_p	mm	85
h_p	mm	128
θ	°	69.37
k	N/mm	6.56

3.4 Defect Size Analysis

As shown in Figure 16 and Figure 17, the schematic diagram of the ultrasonic flaw detection is arranged symmetrically along the weld seam, and the ultrasonic waves are scattered at a certain angle through the probe wedge block after being emitted through the wafer[10]. The closest distance between the two probes is the surface wave, and the backwall wave is reflected by the bottom surface. If there is a defect in the weld, the wave will be diffracted at the upper and lower boundaries of the defect to form diffracted waves.

The speed of sound in steel is C_L, The transit time of the surface wave can be determined as:

$$t_{st} = \frac{2S}{C_L} + 2t_0 \tag{10}$$

The large spherical tank has a large radius of curvature, and the surface is approximately a plane. The distance from the defect to the wall surface is approximately the shortest distance to the surface wave. From the triangle geometry we can know that:

$$t_{di} = 2\left(\frac{\sqrt{S^2 + d_i^2}}{C_L} + t_0\right) \tag{11}$$

Authorized licensed use limited to: Massey University. Downloaded on August 08,2020 at 23:15:40 UTC from IEEE Xplore. Restrictions apply.

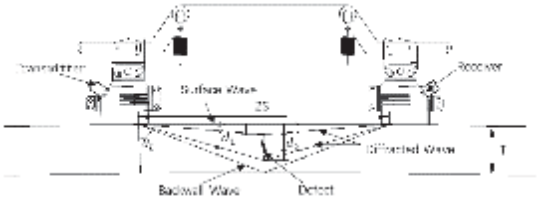

Figure 16. Detection schematic

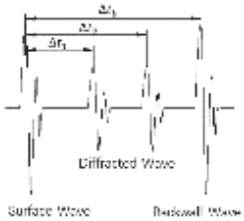

Figure 17. Wave form

The distance between the upper and lower boundaries of the defect to the wall surface can be determined as:

$$d_i = \sqrt{\frac{1}{4}(C_L \Delta t_i)^2 + C_L \Delta t_i S} \tag{12}$$

Then the length of the defect is:

$$L_f = d_2 - d_1 \tag{13}$$

4 Experiment

The arrangement of the experimental site is shown in Figure 18. The wall-climbing robot is attached to the wall for work. The laser tracker is used to locate and track the robot. The computer is used for robot control and laser tracker tracking analysis. The router acts as a base station to realize wireless communication between the computer and the robot. The installation position of the ultrasonic probe is shown in Figure 19. Figure 20 shows the adaptation of curved surfaces.

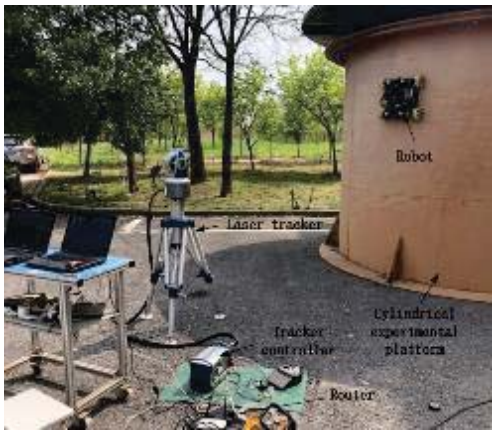

Figure 18. Arrangement of the experimental site

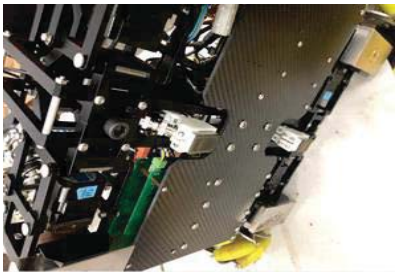

Figure 19. Probe installation

Figure 20. Adaptation of curved surfaces

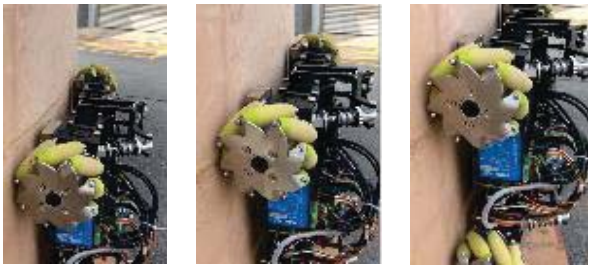

Figure 21. The process of crossing the weld

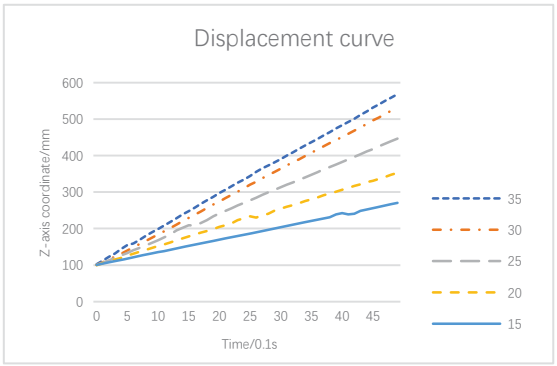

Figure 22. Displacement curve in the z direction

According to the design requirements, the trolley needs to be able to cross the weld height of 4mm, and the constant speed of the trolley is made to pass over the weld seam. Figure 21 shows the process of crossing the weld seam. The car can be smoothly adsorbed to the wall during the entire obstacle crossing process. The car crawls over the weld at different speed factors, and the displacement curve in the vertical direction is shown in Figure 22.

Authorized licensed use limited to: Massey University. Downloaded on August 08,2020 at 23:15:40 UTC from IEEE Xplore. Restrictions apply.

It can be seen from the curve that the speed of the vertical direction does not decrease significantly when the vehicle crosses the obstacle at different speeds. When the car crosses the obstacle at a lower speed, the displacement curve at the obstacle is slightly dithered. Therefore, avoiding the selection of a lower speed allows the robot to cross the obstacle without affecting the running speed and increase the stability of the robot wall climbing motion.

The typical waveform obtained from experiments on the experimental platform is shown in Figure 23. If there is a defect in the weld, two diffracted wave will appear between the surface wave and the bottom wave. The defect size can be found according to (12) and (13).

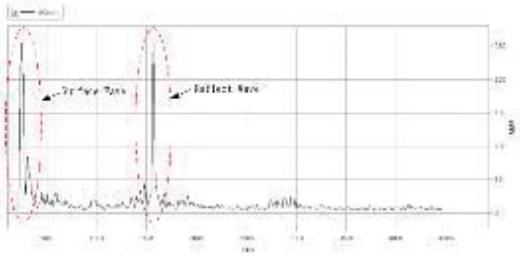

Figure 23. Typical wave form

5 Conclusion

In this paper, a wall climbing robot is designed for the detection of spherical tank welds. The robot was analyzed for the external structure of the spherical tank. According to the experiment, the robot can better adapt to the spherical surface with different curvatures, and can overcome obstacles such as welds on the surface. This paper verifies the feasibility of automatic testing of wall-climbing robots on spherical tanks.

Acknowledgment

This partly supported by the Jiangsu Major Research and Development (Social Development) project no.BE2016802.

References

[1] Fehrenbacher, Axel , et al. "Effects of tool–workpiece interface temperature on weld quality and quality improvements through temperature control in friction stir welding." The International Journal of Advanced Manufacturing Technology 71.1-4(2014):165-179.

[2] Thomas, C. , et al. Ensuring Human Safety with Offline Simulation and Real-time Workspace Surveillance to Develope a Hybrid Robot Assistance System for Welding of Assemblies. Enabling Manufacturing Competitiveness and Economic Sustainability. Springer Berlin Heidelberg, 2012.

[3] Kalra, Love P , J. Gu , and M. Meng . "A Wall Climbing Robot for Oil Tank Inspection." IEEE International Conference on Robotics & Biomimetics IEEE, 2007.

[4] Nishi, A., and H. Miyagi. "Control of a wall-climbing robot using propulsive force of propeller." International Conference on Advanced Robotics, 1991.

[5] Kim, Hwang , et al. "Development of a wall-climbing robot using a tracked wheel mechanism." Journal of Mechanical Science & Technology 22.8(2008):1490-1498.

[6] Nishi, Akira . "A biped walking robot capable of moving on a vertical wall." Mechatronics 2.6(1992):543-554.

[7] Tavakoli, Mahmoud , et al. "OmniClimbers: Omni-directional magnetic wheeled climbing robots for inspection of ferromagnetic structures." Robotics and Autonomous Systems 61.9(2013):997-1007.

[8] Chu, Baeksuk , and Y. W. Sung . "Mechanical and electrical design about a mecanum wheeled omni-directional mobile robot. " International Conference on Ubiquitous Robots & Ambient Intelligence IEEE, 2013.

[9] Da Silva, Marcus, et al. "Directed wireless communication." U.S. Patent No. 8,412,106. 2 Apr. 2013.

[10] Lu, Cheng, Q. Wang, and F. N. Liu. "Ultrasonic TOFD in the Application of Thick Wall Tube Welding Seam Detection Pre-Research." Advanced Materials Research 912-914(2014):12-17.

Jie LI: Male, Doctoral candidate, Mobile and inspection robot, College of Mechanical Engineering, Southeast University, Nanjing, China, 17625356432

Authorized licensed use limited to: Massey University. Downloaded on August 08,2020 at 23:15:40 UTC from IEEE Xplore. Restrictions apply.